Inorg. Chem. **2007**, *46*, 2067–2079

Experimental and Theoretical Methods to Investigate Extraframework Species in a Layered Material of Dodecaniobate Anions

May Nyman,*,† James P. Larentzos,†,‡ Edward J. Maginn,‡ Margaret E. Welk,† David Ingersoll,† Hyunsoo Park,§ John B. Parise,§ Ivor Bull,|| and François Bonhomme†,⊥

Sandia National Laboratories, Albuquerque, New Mexico 87185, Department of Chemical and Biomolecular Engineering, University of Notre Dame, Notre Dame, Indiana 46556, and the Department of Chemistry, Department of Geosciences, Center for Environmental Science, SUNY, Stony Brook, Stony Brook, New York 11794

Received August 2, 2006

The highly charged dodecaniobate Keggin ions $[XNb_{12}O_{40}]^{-16}$ (X = Si, Ge) and $[XNb_{12}O_{40}]^{-15}$ (X = P) serve as building blocks of self-assembled, low-dimensional anionic framework materials. In addition to its high charge, the Keggin ion provides optimal binding geometries that render these materials as attractive metal sorbents and ion exchangers. We describe here the synthesis and single-crystal X-ray structure of $K_{10-x}[Nb_2O_2][H_xGeNb_{12}O_{40}]\cdot 11H_2O$ ($GeNb_{12}$-2d; $x = \sim 1–1.5$), a phase featuring 2D linkage of $[GeNb_{12}O_{40}]^{-16}$ Keggin ions interlayered with charge-balancing K^+ cations and water molecules. Thermogravimetry, infrared spectroscopy (IR), ^1H MAS NMR, and D_2O exchange experiments as well as computational studies were used to describe the location and behavior of these interlayer, extraframework species. To model the basicity of the different types of framework oxygen sites appropriately, atomic-centered partial charges were derived from density functional theory (DFT) calculations to model the electrostatic potential. This model enabled the locations and bonding of K^+ cations associated with the framework, as well as K^+ cations bound predominantly to water in the interlayer space, to be accurately computed via Monte Carlo simulation. The poorest agreement between experimental and simulation results was observed for potassium sites that were associated with disordered portions of the framework, namely, the $[Nb_2O_2]^{6+}$ bridge between Keggin ions. Finally, through grand canonical Monte Carlo (GCMC) calculations, saturation water loadings consistent with experimental measurements were computed.

Introduction

The vast range of metal oxide open-framework materials generally include aluminosilicate zeolites,[1–3] alumino-[6] and metalaluminophosphates,[3–5] octahedral,[6,7] mixed octahedral–tetrahedral,[8] and mixed octahedral–pentahedral–tetrahedral[9] frameworks, clays,[10] and other layered structures.[11,12] Open-framework materials have found uses in numerous applications including ion,[13–18] gas, and molecule separations[19–21] and catalysis.[22–25] The affectivity of these functional materi-

* To whom correspondence should be addressed. E-mail: mdnyman@sandia.gov.
† Sandia National Laboratories.
‡ University of Notre Dame.
§ SUNY, Stony Brook.
|| Present address: Engelhard Corporation R&D, Iselin, New Jersey 08830.
⊥ Present address: Ecole Centrale de Paris, Laboratoire SPMS, 92295 Chatenay-Malabry, France.

(1) Cundy, C. S.; Cox, P. A. *Microporous Mesoporous Mater.* **2005**, *82*, 1–78.
(2) Cundy, C. S.; Cox, P. A. *Chem. Rev.* **2003**, *103*, 663–701.
(3) Cheetham, A. K.; Ferey, G.; Loiseau, T. *Angew. Chem., Int. Ed.* **1999**, *38*, 3268–3292.
(4) Pastore, H. O.; Coluccia, S.; Marchese, L. *Ann. Rev. Mater. Res.* **2005**, *35*, 351–395.
(5) Yu, J. H.; Xu, R. R. *Acc. Chem. Res.* **2003**, *36*, 481–490.
(6) Brock, S. L.; Duan, N. G.; Tian, Z. R.; Giraldo, O.; H, H. Z.; Suib, S. L. *Chem. Mater.* **1998**, *10*, 2619–2628.
(7) Nyman, M.; Tripathi, A.; Parise, J. B.; Maxwell, R. S.; Harrison, W. T. A.; Nenoff, T. M. *J. Am. Chem. Soc.* **2001**, *123*, 1529–1530.
(8) Rocha, J.; Anderson, M. W. *Eur. J. Inorg. Chem.* **2000**, 801–818.
(9) Rocha, J.; Lin, Z. *Rev. Mineral. Geochem.* **2005**, *57*, 173–201.
(10) Kloprogge, J. T. *J. Porous Mater.* **1998**, *5*, 5–41.
(11) Rives, V.; MA, M. A. U. *Coord. Chem. Rev.* **1999**, *181*, 61–120.
(12) Sels, B. F.; Vos, D. E. D.; Jacobs, P. A. *Catal. Rev. Sci. Eng.* **2001**, *43*, 443–488.
(13) Tripathi, A.; Medvedev, D. G.; Nyman, M.; Clearfield, A. *J. Solid State Chem.* **2003**, *175*, 72–83.
(14) Anthony, R. G.; Dosch, R. G.; Philip, C. V. Method of Using Novel Silico-titanates. U.S. Patent No. 6,110,378, Sandia National Laboratories, 2000.
(15) Anthony, R. G.; Philip, C. V.; Dosch, R. G. *Waste Manage.* **1993**, *13*, 503.

10.1021/ic061454l CCC: $37.00
Published on Web 02/14/2007

als is improved by high surface-area (small grain size) and a network of pores, channels, or layers that is readily accessible to the surrounding medium. These networks contain mobile cations including alkali or alkaline earth metals, alkylammonium cations, or hydronium cations, with water molecules coordinating the cations and stabilizing the channel pores or layers through hydrogen bonding and space filling. The location, mobility, and chemical behavior (i.e., acid−base characteristics) of these extraframework species strongly influence the material behavior and functionality. However, the exact nature of these species is difficult to characterize by standard methods such as NMR or vibrational spectroscopies or by crystal structure analysis, given their highly mobile and fluxional nature that frequently results in partial or mixed occupancy of crystallographic sites.

We are particularly interested in anionic framework materials as cation exchangers in which the behavior of both the extraframework species and the geometry of the framework defines selectivity, kinetics, and capacity of cation exchange. Currently, we are investigating the ion-exchange behavior of materials composed of $[XNb_{12}O_{40}]^{16-}$ (X = Si, Ge) or $[XNb_{12}O_{40}]^{15-}$ (X = P) Keggin ion clusters linked in one dimension by $[Ti_2O_2]^{4+}$ or $[Nb_2O_2]^{6+}$ bridges.[26,27] The chains have an overall charge of −10 to −12 that is balanced with hydrated sodium or potassium cations. The chains are not linked to each other except through these mobile species. Attractive features of these phases as ion-exchange materials include stability in basic media, the flexibility and accessibility of the channels between the framework chains, the high negative charge of the framework, and ideal cation binding geometries of the Keggin ions, such as the "windows" in which a cation can coordinate to four framework oxygen atoms.[26]

Computational studies are complementary to experimental methods for locating and describing the geometry of extraframework species based on space-filling requirements and optimal interactions between the framework, the cations, and the water molecules. For instance, in a prior study,[26] we were able to locate only one third of the water molecules by powder X-ray diffraction in isostructural Keggin chain phases $Na_{12}[Ti_2O_2][XNb_{12}O_{40}]\cdot xH_2O$ and $Na_{10}[Nb_2O_2][XNb_{12}O_{40}]\cdot xH_2O$ (X = Si, Ge). The remaining highly mobile water molecules were detected experimentally by thermogravimetry, and computational studies proved these additional highly mobile water molecules could, in fact, be accommodated in the interchain regions. Snapshots of possible geometric arrangements of these water molecules were also described by computational studies. Furthermore, the computationally determined sodium sites agreed well with those located by crystallographic methods for $Na_{12}[Ti_2O_2][SiNb_{12}O_{40}]\cdot xH_2O$, and although we were unable to determine which sodium sites depopulated for charge-balancing requirements of isostructural $Na_{10}[Nb_2O_2][SiNb_{12}O_{40}]\cdot xH_2O$, computational methods produced a chemically and structurally reasonable model.

In this prior study, the computational models could be only partially validated by experimental data because of the microcrystalline character of the samples and the highly mobile nature of the water molecules. In the present study, we report the synthesis and structural characterization of a related dodecaniobate Keggin ion phase, $K_{10-x}[Nb_2O_2][H_xGeNb_{12}O_{40}]\cdot 11H_2O$ ($GeNb_{12}$-2d; $x = \sim 1-1.5$), a 2D network of dedecaniobate Keggin ions that features relatively immobile extraframework species and that could be grown as better quality crystals. These characteristics provided an opportunity to identify by X-ray diffraction all of the alkali cations and all of the water molecules (on the basis of agreement with TGA) and thus proved a better system to validate our computational methods for predicting the behavior and location of these extraframework species. Yet, partial occupancies and mobility of K^+ and H_2O offer sufficient complexity to the system so that it might be modeled and interpreted in multiple ways. We have used other experimental methods including D_2O exchange, ^1H MAS NMR, and infrared spectroscopy to characterize these extraframework species. To complement the experiments, classical Monte Carlo simulations are conducted to provide a detailed molecular-level description of the adsorption behavior of water, along with calculations of the preferred cation and water locations in $GeNb_{12}$-2d. Efficient sampling algorithms, such as replica exchange Monte Carlo simulations (REMC) were required to probe configuration space for this material adequately.

An additional focus of this article is to report a new structure of linked dodecaniobate Keggin ions. The Keggin chains are linked in the orthogonal direction by potassium cations to produce a layered structure. This phase continues to illustrate the tendency of the dodecaniobate Keggin ion and its lacunary derivatives[28] to serve as discrete, highly charged building blocks for self assembly of complex materials.

Experimental Section

Synthesis of $K_{10-x}[GeNb_{12}O_{40}][Nb_2O_2]\ 11H_2O$ ($x = \sim 1-1.5$; $GeNb_{12}$-2d). In a 100 mL Teflon liner for a Parr reactor, we dissolve 1.1 g (19.6 mmol) of KOH pellets in a mixture of 40 mL of deionized water and 10 mL of ethylene glycol. While stirring, 1.75 g amorphous, hydrated niobium oxide (9.2 mmol Nb, assuming

(16) Behrens, E. A.; Sylvester, P.; Clearfield, A. *Environ. Sci. Technol.* **1998**, *32*, 101−107.
(17) Kesraouiouki, S.; Cheeseman, C. R.; Perry, R. *J. Chem. Technol. Biotechnol.* **1994**, *59*, 121−126.
(18) Sylvester, P.; Clearfield, A. *Solvent Extr. Ion Exch.* **1998**, *16*, 1527−1539.
(19) Flanders, C. L.; Tuan, V. A.; RD, R. D. N.; Falconer, J. L. *J. Membr. Sci.* **2000**, *176*, 43−53.
(20) Poshusta, J. C.; Tuan, V. A.; Pape, E. A.; Noble, R. D.; Falconer, J. L. *AIChE J.* **2000**, *46*, 779−789.
(21) Javaid, A. *Chem. Eng. J. (Amsterdam, Neth.)* **2005**, *112*, 219−226.
(22) Corma, A. *J. Catal.* **2003**, *216*, 298−312.
(23) Yu, J. H.; Xu, R. R. *Acc. Chem. Res.* **2003**, *36*, 481−490.
(24) Ozin, G. A. *Adv. Mater. (Weinheim, Ger.)* **1994**, *6*, 71−76.
(25) Dag, O.; Kuperman, A.; Ozin, G. A. *Adv. Mater. (Weinheim, Ger.)* **1995**, *7*, 72−78.
(26) Bonhomme, F.; Larentzos, J. P.; Alam, T. M.; Maginn, E. J.; Nyman, M. *Inorg. Chem.* **2005**, *44*, 1774−1785.
(27) Nyman, M.; Bonhomme, F.; Alam, T. M.; Rodriguez, M. A.; Cherry, B. R.; Krumhansl, J. L.; Nenoff, T. M.; Sattler, A. M. *Science* **2002**, *297*, 996−998.
(28) Nyman, M.; Celestian, A. J.; Parise, J. B.; Holland, G. P.; Alam, T. M. *Inorg. Chem.* **2006**, *45*, 1043−1052.

~30 wt % water in the niobium oxide), and 1.65 g of tetraethoxygermanium (6.5 mmol $Ge(OC_2H_5)_4$) are added and stirred for 20 min. The pH of the mixture is 11.5. The Teflon liner is enclosed in its autoclave and placed in a 195 °C oven for 8−15 h. Approximately 0.18−0.35 g of microcrystalline white powder is collected (yield ~10−20% based on Nb). The water content was determined by TGA: 7.5 wt % volatile portion, which translates to approximately 11 molecules of water per formula unit. Composition analysis (calculated on the basis of 11 water molecules per formula unit, 8.8 K^+ cations determined from X-ray structure) yielded the following: Nb: 48.9 wt % calcd, 46.4 wt % found. K: 13.4 wt % calcd, 13.7 wt % found. Ge: 2.9 wt % calcd, 2.6 wt % found. By EDS (energy dispersive spectroscopy), no other common alkali cations such as sodium are detected.

D_2O Exchange. The $GeNb_{12}$-2d powder (~1 g) for D_2O exchange was placed in a conical 15 mL centrifuge tube, and ~10 mL D_2O (99.8%, Alfa-Johnson-Matthey) was added. The centrifuge tube was capped and shaken to obtain a slurry and left to sit at room temperature for 30 min. (This process was also carried out at elevated temperature, 50 °C, but did not result in more complete D_2O exchange.) The slurry was then centrifuged down, and the majority of the liquid was decanted off. This process was repeated a total of four times. After the final D_2O contact, the centrifuge tube containing the wet powder was placed in a vacuum oven and dried in vacuo at 40 °C overnight. The D_2O-exchanged powder was handled and stored for extended periods in a controlled-atmosphere glove box to avoid back exchange with atmospheric H_2O.

Instrumentation. $GeNb_{12}$-2d was characterized by powder X-ray diffraction, thermogravimetry (TGA-DTA), compositional analysis, infrared spectroscopy (IR), and ^1H solid-state MAS NMR spectroscopy (magic angle spinning nuclear magnetic resonance). Powder X-ray diffraction was carried out with a Bruker D8 Advance diffractometer in Bragg−Brentano geometry with Ni-filtered Cu Kα radiation. Thermogravimetry was performed on a TA Instruments SDT 2960 with an 8.7 mg sample size and heated at 5 °C/min under nitrogen flow up to 850 °C. Compositional analysis on Ge, Nb, and K was carried out by Galbraith Laboratories, Inc. (Knoxville, TN). Infrared spectra (400−4000 cm^{-1}) were collected on a Thermo Electron Corp. Nicolet 380 FTIR using a Diamond single-bounce ATR configuration. ^1H NMR spectra were performed on a Bruker Avance 600 operating at a proton frequency of 600.1 MHz using a 2.5 mm broadband double-resonance probe spinning at 20 kHz. Intensities were given as ratios against the sample weight within the rotor.

Impedance Measurements. Impedance measurements of free-standing pellets were made using a Schlumberger 1255 Frequency Response Analyzer, a 1287A potentiostat, and Z-plot software. Pressed pellets were wetted using a known quantity of 18 MΩ water placed onto the center and perimeter of the pellet. The pellet was placed between gold electrodes, and compression was applied shortly after wetting the pellet to make contact with the oxide and to maintain the mechanical integrity of the pressed disc. Measurements were made over a frequency range of 100 kHz to 0.1 Hz using a 10 mV applied ac signal. The fixture used for holding the gold electrodes allowed for in situ measurement of the sample thickness. The electrode diameter was 2.98 cm. All of the measurements were made at room temperature. Free-standing pellets of the oxide were prepared by placing a known quantity of dry material into a pellet press and applying 102 lbs·in^{-2} for 30−120 s at room temperature.

Single-Crystal X-ray diffraction. The small size of the crystals did not permit structure characterization using an in-house diffractometer. Data collection and structure determination were carried out using a 15-ID ChemMatCARS beamline equipped with a Bruker 6000 CCD detector at Advanced Photon Source, Argonne National Laboratory. The data were collected at 77 K with a wavelength of 0.4959 Å with an exposure time of 1 s/frame and a detector distance of 5.0 cm. Data were collected down to a resolution of 0.75 Å. Two major sections of frames were collected with a step size of 0.30° in ω and ϕ. The raw intensity data were collected and integrated with software packages SMART and SAINT. Then, an empirical absorption correction was applied using SADABS. The crystal structure was solved via a direct method and refined assuming anisotropical displacement parameters for all atoms with SHEXTL. Framework metal atoms were located first, and the remaining atoms were found from subsequent Fourier difference map synthesis.

Molecular Modeling. Classical simulation methods were extended to GeNb12-2d, where the interatomic potentials are described through a pairwise additive short-range 12−6 Lennard-Jones potential and a long-range Coulomb potential, as given by the expression

$$U_{ij} = 4\epsilon_{ij}\left[\left(\frac{\sigma_{ij}}{r_{ij}}\right)^{12} - \left(\frac{\sigma_{ij}}{r_{ij}}\right)^{6}\right] + \frac{q_i q_j}{4\pi\epsilon_0 r_{ij}} \quad (1)$$

where r_{ij} is the separation distance between atoms i and j, σ_{ij} represents the collision diameter, ϵ_{ij} is the well depth, ϵ_0 is the permittivity of vacuum, and q_i is the charge on atom i. The Kiselev[29] convention is used for the short-range repulsion−dispersion interactions, where the oxygen atoms of the framework are assumed to shield the effects of the remaining framework atoms. Thus, only the K^+-O_{water}, $K^+-O_{framework}$, water−water, and $O_{water}-O_{framework}$ parameters are required for the short-range repulsion−dispersion model. The water molecules are modeled with a rigid simple point charge (SPC)[30] water model, which has pure-component Lennard−Jones parameters of $\sigma_{ij} = 3.169$ Å and $\epsilon_{ij}/k_B = 78.201$ K and partial charges of $q_O = -0.82$ and $q_H = +0.41$. Following the modeling approach for the interaction of various water models with montmorillonite,[31,32] the pure component SPC water parameters are extended to the water−$O_{framework}$ interaction without modification. Finally, the pure-component potassium parameters[33] are $\sigma_{ij} = 3.250$ Å and $\epsilon_{ij}/k_B = 63.734$ K. The Lorentz−Berthelot combining rules are used to obtain the cross interactions.

To improve upon a previously used potential model for polyoxoniobates,[26] partial charges are extracted from density functional theory (DFT) simulations and are placed at the atomic centers to model the electrostatic potential. Plane wave DFT simulations using the Vienna ab initio simulation package (VASP)[34] are conducted to determine the minimum-energy structure of GeNb12-2d. Core electronic states are described using the accurate projector-augmented wave (PAW) approach, electron exchange and correlation are treated within the generalized gradient approximation (GGA), and plane waves are included up to a 400 eV energy cutoff.[35] A 2 × 2 × 4 Monkhorst−Pack mesh is used to sample the first Brillouin zone. For the DFT calculations, one unit cell of

(29) Kiselev, A. V.; Lopatkin, A. A.; Shulga, A. A. *Zeolites* **1985**, *5*, 261−267.
(30) Berendsen, J. J. C.; Postma, J. P. M.; Gunsteren, W. F. v.; Hermans, J. *Intermolecular Forces*; Reidel: Dordrecht, Holland, 1981.
(31) Boek, E. S.; Coveney, P. *Langmuir* **1995**, *11*, 4629−4631.
(32) Whitley, H. D.; Smith, D. E. *J. Chem. Phys.* **2004**, *120*, 5387−5395.
(33) Rajamani, S.; Ghosh, T.; Garde, S. *J. Chem. Phys.* **2004**, *120*, 4457−4466.
(34) Kresse, G.; Furthmuller, J. *Comput. Mater. Sci.* **1996**, *6*, 15−50.
(35) Kresse, G.; Joubert, J. *Phys. Rev. B, Condens. Matter Mater. Phys.* **1999**, *59*, 1758.

Table 1. Summary of Crystallographic Data for $GeNb_{12}$-2d

formula	$H_{26}O_{55}K_{10}GeNb_{14}$
formula weight	2670.6
space group	orthorhombic *Imm*2
unit cell parameters	$a = 10.958(2)$ Å
	$b = 11.553(2)$ Å
	$c = 19.983(4)$ Å
V	2529.9(9) Å^3
Z	2
density (calcd)	3.640 g/cm^3
synchrotron radiation	0.49594 Å
exptl abs coeff, μ	10.309
temperature	100 K
2θ min, max	2.84°, 38.46°
morphology	block
color	colorless
crystal dimensions	$0.03 \times 0.03 \times 0.02$ mm^3
measured reflections	3148
independent reflections	2922
reflections with $>2\sigma$(I)	2736
R1 [$F^2 > 2\sigma(\mathbf{F}^2)$]	5.43
R1 (all data)	5.43
wR2 (all data)	14.93
GOF	1.086
parameters refined	157

Table 2. Partial Charge of Atoms for Computational Model for GeNb12-2d

atom type	charges
Ge	1.940
Nb	3.270
O_t (Keggin)[a]	−1.150
O_b (bridge; $\mu-2$)[b]	−1.520
O_c (Keggin)[c]	−1.520
O_b (Keggin; $\mu-2$)	−1.520
O_b (Keggin; $\mu-3$)	−1.520
K^+	1.000
O_{water}	−0.820
H_{water}	0.410

[a] t = terminal oxygen, double bonded to Nb in the Keggin ion. Bridging oxygens are found in the $[Nb_2O_2]$ unit (bridge) or Keggin. [b] b = bridging oxygen ($\mu-2$ or $\mu-3$). [c] c = central oxygen bonded to Ge.

the *dehydrated* GeNb12-2d structure is modeled with the framework atoms and counterbalancing potassium cations constrained to their experimentally determined positions (Supporting Information). The Wigner−Seitz analysis method is used to extract the partial charges from the DFT simulations, which are given in Table 2. A full description of the Wigner−Seitz methodology for charge extraction from plane wave DFT simulations is given elsewhere.[36]

An examination of the partial charges in Table 2 indicates that the framework oxygen atoms vary depending on the coordinating environment. Five distinct oxygen atom types have been distinguished, as noted in Table 2. In previous studies,[26] we assumed that the oxygen charge was uniform over all of the oxygen atoms in the system. However, through DFT simulations, it is clearly shown that the terminal oxygen atoms are more positive (less basic) than the remaining four oxygen atom types.

Grand canonical Monte Carlo (GCMC) simulations and canonical replica exchange Monte Carlo (REMC) simulations are conducted to simulate GeNb12-2d and are described in detail in the Appendix. All of the simulations are performed with a locally developed software package. Full periodic boundary conditions were employed with an interaction cutoff of 9.5 Å. The long-range Coulombic interactions were evaluated using the Ewald summation method.[37]

(36) Larentzos, J. P.; Schneider, W. F.; Maginn, E. J. Submitted to *J. Phys. Chem. B*, 2006.
(37) Allen, M. P.; Tildesley, D. J. *Computer Simulation of Liquids*; Clarenden: New York, 1989.

Configurations from the Monte Carlo trajectories containing the instantaneous positions of the potassium cations and water molecules were output every 2000 Monte Carlo steps. An analysis of these configurations yields the preferred adsorption sites for potassium and water in GeNb12-2d. Following the approach used in our previous studies,[26] a potassium cation or water molecule is considered to be associated with an experimental site if it is located within 2.0 Å of any of the site's crystallographically equivalent positions. In analyzing each configuration, we also compute the fraction of time that a particular experimental site is associated with a given cation or water molecule, which we refer to hereafter as the "population fraction". This is conceptually related to the experimental occupancy. Upon assigning the cation or water molecule to a particular site, the *Imm*2 symmetry operations are applied to determine the asymmetric coordinate of each cation or water molecule. Finally, an average over all of the asymmetric coordinates gives the simulated coordinates of the cation or water molecule, which can be further compared with the experimental X-ray diffraction sites. Because there are no symmetry constraints during the simulations, the potassium cations and water molecules tend to be located in sites that are slightly removed from sites with higher point symmetry. As described in our previous studies,[26] we have reported the raw averaged coordinates and the idealized coordinates that are obtained by shifting the raw averaged coordinates onto nearby sites with higher point symmetry.

Results and Discussion

Synthesis. The synthesis, chemical behavior, and structure of $GeNb_{12}$-2d resemble previously reported phases that feature linked dodecaniobate α-Keggin ions. In particular, the successful formation of $GeNb_{12}$-2d proved to be quite sensitive to both processing conditions and reagents. The extremely low yield (around 10−20%) of $GeNb_{12}$-2d is reminiscent of the formation of the previously reported Keggin chain materials that featured α-$[TNb_{12}O_{40}]^{16-}$ (T = Si, Ge) ions linked in one dimension by $[Nb_2O_2]^{6+}$ bridges and charge balanced by hydrated sodium cations.[26] We attribute the low yield to the lability of the $[Nb_2O_2]^{6+}$ bridges because comparable linked Keggin ion materials featuring $[Ti_2O_2]^{4+}$ bridges are more robust compounds that can be synthesized in higher yields (60−90%). Without the more inert $[Ti_2O_2]^{4+}$ bridges, a higher concentration of the Keggin clusters is retained in solution rather than precipitated into the solid phase. The robustness of these phases is judged by their ability to withstand ion exchange, heat, X-rays, or time without the degradation of long-range order. Some variations in chemical reagents were made, and these syntheses did not produce $GeNb_{12}$-2d. For example, carrying out the reaction in just water instead of a water/ethylene glycol mix produced no precipitate. The ethylene glycol apparently serves to decrease the polarity of the solution and allow condensation of the Keggin ions into the 2D network. However, ethylene glycol cannot be universally applied to aid in the precipitation of hetreopolyniobate phases; on the contrary, other nonaqueous solvents cannot be substituted for ethylene glycol to obtain the same results. If we eliminate the ethylene glycol and instead increase the niobium concentration to favor the precipitation of solids, amorphous powders are obtained. If the synthesis is carried out with silicon instead of germanium for the central TO_4 site, the

Table 3. Selected Bonds Lengths (Å) and Angles (deg) in the $[K][Nb_2O_2][GeNb_{12}O_{40}]^{10-}$ Framework

atom A	atom B	atom C	bond length (Å) (atom A−atom B)	bond angle (deg) (atom A−atom B−atom C)
O_c13[a]	Ge1	O_c13	1.76(2)	109.5(14)
O_c14		O_c14	1.68(3)	108(2)
O_c13		O_c14		111.6(9), 108.1(9)
O_b8[b]	K1	2.85(1)	O_b8	127.1(7), 105.1(6)
O_b9		2.89(1)	O_b8	86.0(4), 122.4(3)
O_b9			O_b9	82.8(5), 116.8(6)
O_b1 (bridge)[c]	Nb1(bridge)	O_b2	2.00(2)	72(1)
O_b2 (bridge)[c]		O_b3	1.83(3)	76(1), 109(2)
O_b3 (Keggin)[d]		O_b1	1.97(1)	109.8(8)
O_b4 (Keggin)[d]		O_b1	2.06(1)	113.9(7), 88.7(6)
O_b2		O_b4		118(2)
O_b3		O_b3		84.1(7)
O_b3		O_b4		122.6(6), 78.0(4)
O_b4		O_b4		67.8(6)
O_t5[e]	Nb2	O_b12	1.86(2)	93.5(5)
O_b12		O_b4	1.99(1)	87.0(4)
O_b4		O_t5	1.99(1)	104.7(7)
O_c14		O_b12	2.47(3)	111.9(8), 72.4(8)
O_b4		O_b4		70.3(6)
O_b4		O_c14		83.3(8)
O_b12		O_b12		111.1(6)
O_t15	Nb3	O_b6	1.70(2)	117.1(6), 105.6(7)
O_b6		O_b3	1.83(1)	99.8(4)
O_b3		O_t15	2.24(1)	95.1(7), 85.2(6)
O_c13		O_b6	2.38(2)	91.9(6)
O_b3		O_c13		97.9(6)
O_b3		O_b3		72.3(6)
O_b6		O_b6		79.3(6)
O_t7	Nb4	O_b8	1.702(9)	112.3(7)
O_b8		O_b9	1.83(1)	92.0(6), 95.2(5)
O_b9		O_b4	2.00(1)	90.6(4)
O_b4		O_t7	2.00(1)	106.0(6)
O_b3		O_t7	2.23(1)	91.4(6)
O_c13		O_b8	2.43(2)	61.0(6)
O_c14		O_b8	2.49(3)	91.8(8)
O_b3		O_b8		98.0(5)
O_b3		O_c14		97.5(8)
O_b9		O_c14		72.8(8)
O_b3		O_c13		68.0(6)
O_b4		O_b3		73.3(4)
O_b4		O_c13		80.9(6)
O_b9		O_c13		111.3(6)
O_t10	Nb5	O_b6	1.71(2)	110.1(6)
O_b6		O_t10	1.90(1)	110.1(6)
O_b8		O_t10	1.90(1)	105.8(6)
O_c13		O_b6	2.48(2)	85.9(6)
O_b6		O_b6		69.9(6)
O_b8		O_c13		90.2(6)
O_b6		O_b8		95.6(5)
O_b8		O_b8		76.8(7)
O_t11	Nb6	O_b9	1.75(2)	94.7(7)
O_b9		O_b9	2.09(1)	95.8(6)
O_b12		O_t11	2.11(1)	90.0(6)
O_c14		O_b9	2.46(3)	104.1(8), 72.1(8)
O_b9		O_b12		80.9(4)
O_b12		O_b12		102.0(6)
O_b12		O_c14		104.2(8), 70.7(8)

[a] c = central oxygen. [b] b = bridging oxygen. [c] Oxygen belonging to the $[Nb_2O_2]$ bridge. [d] Oxygen belonging to the Keggin ion. [e] t = terminal oxygen.

addition of titanium for the bridging sites, or both of these changes simultaneously, amorphous powders are again precipitated. The Si analogue of $GeNb_{12}$-2d can be synthesized only as a mixture with previously reported $K_{12}[Ti_2O_2][SiNb_{12}O_{40}]16H_2O$,[27] a 1D phase of Keggin ions linked by $[Ti_2O_2]^{4+}$. The difficulty of obtaining this hypothetical silicon analogue is not understood, especially considering the ease of substitution of Ge^{4+} for Si^{4+} in previously reported dodecaniobate Keggin ion phases.[26,38]

Structural Description. The Anionic Framework. The most relevant bond lengths and angles are summarized in Table 3, and a representation of the structure emphasizing the anionic framework with atom labels is shown in Figure 1. Like several phases that we have reported thus far featuring dodecaniobate α-Keggin ions,[26,38] the central tetrahedron is disordered, with eight half-occupied oxygen atoms around Ge. The Ge−O bond lengths are 1.68(2) and 1.76(3) Å. The Keggin ion NbO_6 octahedra are distorted in the usual fashion of polyoxometalates: $Nb-O_t$ (t = terminal) bond lengths range from 1.70(2) to 1.86(2) Å, $Nb-O_b$ = 1.83(1) to 2.24-

(38) Nyman, M.; Bonhomme, F.; Alam, T. M.; Parise, J. B.; Vaughan, G. M. B. *Angew. Chem., Int. Ed.* **2004**, *43*, 2787−2792.

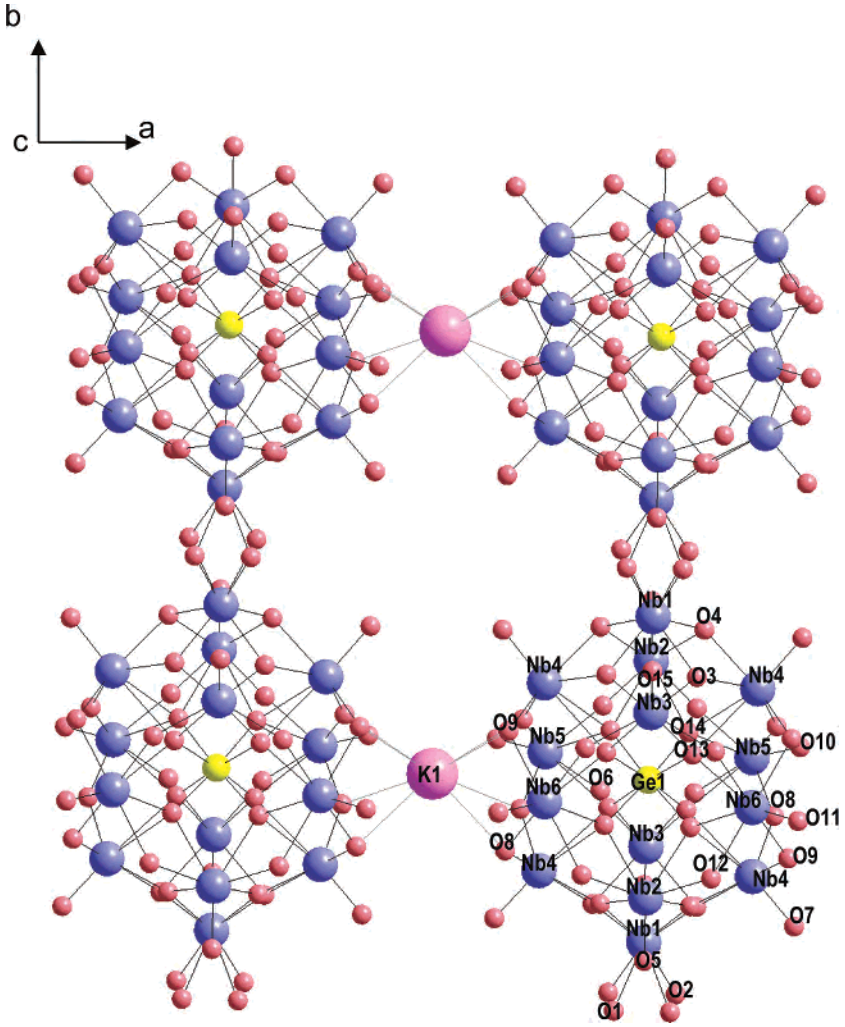

Figure 1. Ball-and-stick model of the framework for $GeNb_{12}$-2d.

(1) Å (O_b are μ-2 or μ-3 bridging oxygens), and the long central Nb−O_c bonds are 2.38(2) to 2.49(3) Å. Along the *b* axis, the $[GeNb_{12}O_{40}]^{16-}$ Keggin ions alternate with $[Nb_2O_2]^{6+}$ units to form infinite chains. This geometry of linked, bicapped Keggin ions has been observed previously in other phases featuring the dodecaniobate Keggin ion,[26,27] a tungstovanadate Keggin ion,[45] and a molybdovanadate Keggin ion.[39,40] The bridging unit can also be described as two edge-sharing NbO_6 octahedra. The shared edge is disordered in two orientations or alternatively described as a square of half-occupied oxygen atoms between two adjacent Nb1 atoms, which has also been observed previously in Keggin chain phases.[26,41] The $[GeNb_{12}O_{40}][Nb_2O_2]^{10-}$ chains are then linked together in the orthogonal direction (along the *a* axis) with K^+ cations that reside between two Keggin ion four-ring windows of neighboring chains. These linking potassium (K1) cations are thus eight-coordinate, with four bonds to O_b8 and four bonds to O_b9 on the order of 2.9 Å. The view down the *b* axis of the $[GeNb_{12}O_{40}][Nb_2O_2]^{10-}$ chains shows each chain to be surrounded by six other chains in a hexagonal arrangement (Figure 2a). This is different from previously reported phases in which each chain is surrounded by four other chains with the straight edges of the Keggin ions facing one another in a checkerboard pattern,[26,40] or each chain is surrounded by four other chains with the corners of the Keggin ions facing one another.[27] The molybdovanadate chain phase reported by Luan et al.[39] also contains hexagonally arranged chains, but the chains are rotated about their axes so the edges of the Keggin ions are not all aligned. The arrangement of the chains relative to one another along the chain axis (*b* axis) is such that two neighboring chains are exactly aligned (along the *a* direction), which allows linking together by the K1 cations, and thus are described as $[K][GeNb_{12}O_{40}][Nb_2O_2]^{9-}$ anionic layers. Figure 2b shows a view along the *c* axis, the stacking direction of the

(39) Luan, G.; Wang, E.; Han, Z.; Li, Y. *Inorg. Chem. Commun.* **2001**, *4*, 541−543.
(40) Muller, A.; Koop, M.; Schiffels, P.; Bogge, H. *Chem. Commun. (Cambridge, U.K.)* **1997**, 1715−1716.
(41) Shivaiah, V.; Hajeebu, S.; Das, S. K. *Inorg. Chem. Commun.* **2002**, *5*, 996−999.
(42) Zawodzinski, T. A.; Neeman, M.; Sillerud, L. O.; Gottesfeld, S. *J. Phys. Chem.* **1991**, *95*, 6040−6044.
(43) Crupi, V.; Majolino, D.; Migliardo, P.; Venuti, V.; Mizota, T. *Mol. Phys.* **2004**, *20*, 1943−1957.
(44) Alam, T. M.; Nyman, M.; Cherry, B. R.; Segall, J. M.; Lybarger, L. E. *J. Am. Chem. Soc.* **2004**, *126*, 5610−5620.
(45) Nyman, M.; Alam, T. M.; Bonhomme, F.; Rodriguez, M. A.; Frazer, C. S.; Welk, M. E. *J. Cluster Science*; web release, 2006, special edition honoring the career of Prof. Michael T. Pope.

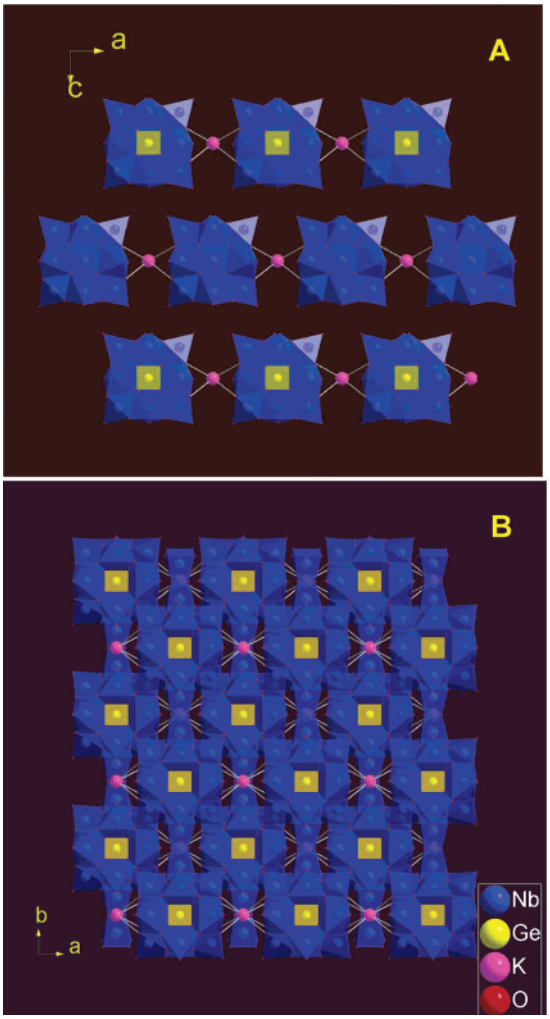

Figure 2. View down the *b* axis showing the relative arrangement of the $[GeNb_{12}O_{40}][Nb_2O_2]^{10-}$ chains (top). View along the *c* axis, the stacking direction of the $[K][GeNb_{12}O_{40}][Nb_2O_2]^{9-}$ layers, emphasizing the offset arrangement of neighboring layers (bottom).

$[K][GeNb_{12}O_{40}][Nb_2O_2]^{9-}$ layers. In this representation, two layers are shown, emphasizing the offset arrangement of neighboring $[K][GeNb_{12}O_{40}][Nb_2O_2]^{9-}$ layers.

Ion Exchange and Conductivity Behavior. $GeNb_{12}$-2d undergoes ion exchange with a variety of metal cations to around 80−90% exchange, as determined by elemental analysis. This is consistent with the exchange of the interlayer potassium cations, that is, all K^+ sites with the exception of K1 that links the 1D Keggin chains into layers. Cations that can be exchanged-in include the alkalis and alkaline earth metals and transition metals such as cobalt and nickel. However, for all of these exchanged-in cations, the exchange process is accompanied by a degree of diminished long-range order of the framework. This is probably because the layers are associated through strong interaction with the interlayer potassium cations. We also characterized the ion conductivity behavior of $GeNb_{12}$-2d via impedance measurements. Figure 3 shows the Nyquist plot for $GeNb_{12}$-2d over a frequency range of 100 kHz to 80 Hz. As seen, these data are well behaved and are linear and near vertical (i.e., normal to the *x* axis) over the range shown, which is close to ideal behavior. Extrapolation of this data to the baseline gives a room-temperature conductivity on the order of 1.3×10^{-3} S·cm. As a basis for comparison, the conductivity of Nafion, the polymer exchange membrane used in fuel cells, is on the order of 10^{-3} S·cm at room temperature.[42] This data clearly indicates the mobility of the potassium cations in the hydrated $GeNb_{12}$-2d.

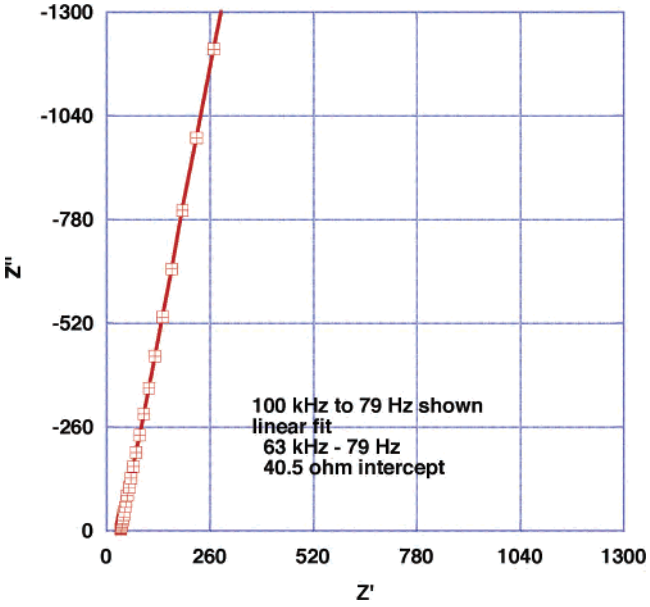

Figure 3. Nyquist plot over the frequency range of 100 kHz to 79 Hz for the free-standing $GeNb_{12}$-2d pellet. Twenty microliters of 18 MΩ water was added to 0.1713 g oxide pellet. Measurement was made at room temperature using gold electrodes.

Extraframework Positions. Potassium Cations. The potassium charge-balancing cations are located on seven crystallographic sites, some necessarily partially occupied as a result of unreasonably close proximity to other crystallographic sites. The total population of potassium is 8.76 per Keggin cluster. We assume the remainder of the charge balance (+1.24) comes from protons on framework oxygen. Bond valence sum calculations plus an inspection of coordination environments of framework oxygens suggest that the O12 oxygen atom of the Keggin cluster is the most reasonable location for protons. The BVS value for O12 is around 1.4, whereas the remainder of the cluster oxygen atoms have BVS values above 1.7. There are four O12 sites per cluster, so disorder of the proton over these four sites is expected. The O12 site is not coordinated to any potassium cations, but it is within hydrogen bonding distance (<3 Å) of two water sites, Ow2 and Ow3. K1, located between two Keggin ions and linking the chains into a 2D network, is considered to be part of the framework and was discussed previously. The disordered oxygens in the $[Nb_2O_2]$ bridge, O1 and O2, are each bonded to two potassium sites: O1 is bonded to K4 and K6, and O2 is bonded to K2 and K7. K2, K4, and K6 are all half-occupied, and K7 is around 40% occupied. The K4−K6 and the K2−K7 distances are around 2.1 Å each and are therefore mutually exclusive in their occupancy. These potassium sites are stabilized by both framework and water oxygens and are octahedrally coordinated. K3 and K5 are similar to one another. Both are fully occupied, residing in the interlayer space and bonded

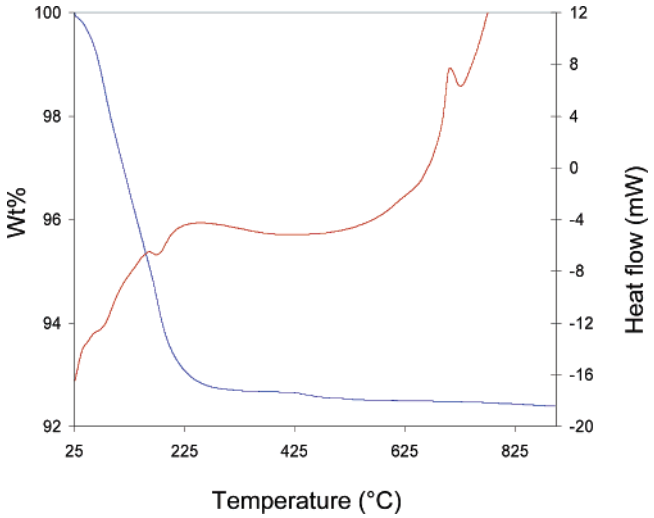

Figure 4. Thermogravimetric (blue) differential thermal analysis (red) of $GeNb_{12}$-2d.

primarily to niobyl oxygen atoms, Nb═O_t, and are also stabilized by lattice water.

Lattice Water. Thermogravimetry, infrared spectroscopy, and ^{1}H MAS NMR of $GeNb_{12}$-2d, before and after D_2O exchange of the lattice water, revealed two distinct populations of water molecules based on relative mobility. The differential thermal analysis curve (DTA) of the TGA-DTA experiment (Figure 4) shows two endothermic weight loss events associated with the loss of lattice water that are centered around 80 and 180 °C, and the total weight loss in this initial part of the TGA curve (up to ~350 °C) is around 7.5%. This corresponds with a molecular formula of around 11 water molecules per Keggin ion. This agrees well with the structural solution that also predicts 11 water molecules per cluster in 6 crystallographic positions. In duplicate experiments, 56% of the $GeNb_{12}$-2d H_2O is exchanged for D_2O, as determined by ^{1}H NMR of the before- and after-exchanged products. This suggests that the amount of exchange is dictated by the mobility of the water molecules within the framework rather than by the purity of the exchanging D_2O, back-exchange with the atmosphere, or other experimental variabilities such as particle size or temperature and time of exchange. Describing 56% of the lattice water as mobile agrees well with the first endotherm of the DTA curve that accounts for the volatilization of roughly half of the lattice water. Figure 5 shows the overlaid ^{1}H MAS NMR spectra of $GeNb_{12}$-2d, before and after D_2O exchange. A simulated deconvolution of $GeNb_{12}$-2d before exchange suggests that there are essentially three broad ^{1}H resonances and two minor sharp resonances. Whereas 56% of the total lattice H_2O exchanges for D_2O, there is clearly preferential exchange of the water molecules giving rise to the broader resonances. This partial and selective exchange of water is also observed by infrared spectroscopy, shown in Figure 6. The $H_2O-GeNb_{12}$-2d sample gives a spectrum with two major and one minor O−H stretching frequencies in the 3200−3600 cm^{-1} region. The two major bands are centered at 3360 and 3200 cm^{-1}. Upon D_2O exchange, the band at 3200 cm^{-1} is diminished, and the D_2O stretching

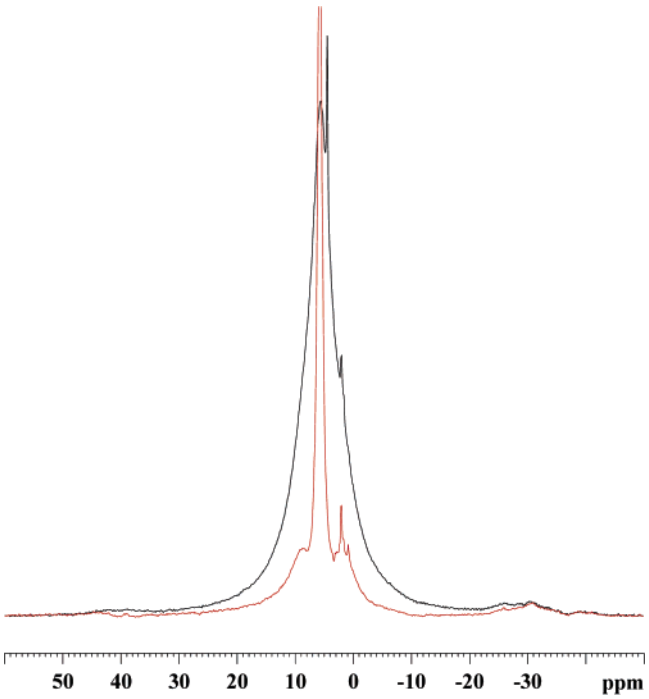

Figure 5. ^{1}H MAS NMR spectra of $GeNb_{12}$-2d before (black) and after (red) exchange of D_2O for H_2O.

and bending frequencies at 2500 and 1450 cm^{-1}, respectively, are observed. This implies that the H_2O population with the 3200 cm^{-1} stretching frequency is more mobile and readily exchanged. A number of vibrational spectroscopy studies have correlated that there is a decrease in the O−H stretch frequency with increased ordering of hydrogen bonding between water molecules (Crupi et al.[43]). A vibrational band around 3200 cm^{-1} has been assigned to water with an ordered network of H-bonding, and a vibrational band around 3400 cm^{-1} is correlated with a less-ordered hydrogen bond network. Ow1 is within H-bonding distance (2.8 Å) of two half occupied and three fully occupied water sites and is not bound to potassium. Ow4 is half occupied and located between two partially occupied K7 sites, forming one bond to K7 and an H-bond to Ow1 and is also within H-bonding distance of two framework oxygens. Ow2 is bound to half-occupied K6 and K4 and fully occupied K3 and iswithin H-bonding range of a framework oxygen. Similarly, Ow3 is bound to partially occupied K2 and K7 and fully occupied K5 and is also in association with the framework. Both Ow5 and Ow6 are hydrogen bonded to framework oxygens only. Ow1, Ow5, Ow4, and Ow6 are expected to be the most mobile water molecules because of their limited coordination to potassium. However, these comprise only 3 of the 11 water molecules per cluster. According to the D_2O exchange experiments and the infrared and NMR spectroscopic analyses, approximately half of the water molecules are readily exchangeable. However, both the Ow2 and the Ow3 sites have two conformations, depending on which of the two mutually exclusive potassium cations are present in the half-occupied sites that are located near these water positions (K4 and K6 for Ow2, K7 and K2 for Ow3). For both Ow2 and Ow3, one environment gives a more bent K−Ow−K

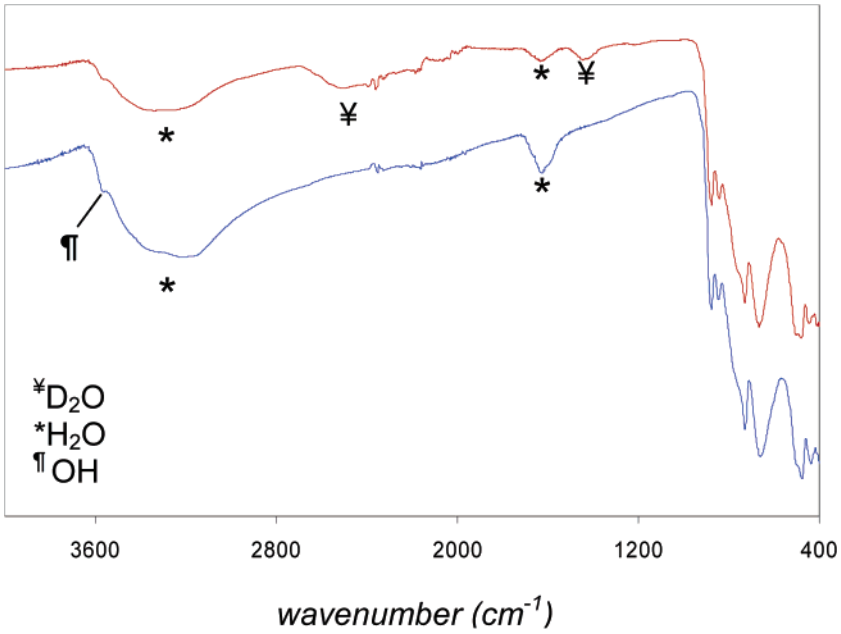

Figure 6. FTIR spectra of $GeNb_{12}$-2d before (blue) and after (red) exchange of D_2O for H_2O.

bond angle, and the other gives a more linear K−Ow−K bond angle. A bent bond angle would likely provide more mobility to the Ow3 and Ow4 water molecule and therefore increase the lability at this site when the appropriate neighboring potassium site is occupied.

The minor O−H resonance at 3600 cm^{-1} is also not diminished by exchange with D_2O. This may be described as an OH belonging to the framework (i.e., Nb_2O_bH, a hydroxyl bridging two cluster oxygen atoms[44]). The small sharp peak at 2 ppm in the ^1H MAS NMR spectrum (that also remains after D_2O exchange) could be consistent with framework-bound hydroxyls. This upfield chemical shift and the inertness of the species relative to exchange are both consistent with a basic bridging hydroxyl of a polyniobate cluster, as has been observed previously for Lindqvist clusters $[HNb_6O_{19}]^{7-}$ and $[H_2Nb_6O_{19}]^{6-}$.[44,45] The thermogravimetric data provided more evidence for framework hydroxyls: the small weight loss around 425 °C can be correlated to a loss of this species (Figure 4). Finally, if the $[Nb_2O_2][GeNb_{12}O_{40}]^{10-}$ framework is partially charge-balanced by protons in the form of OH^- ligands, as well as K^+, there should be fewer than 10 K^+ per Keggin cluster. Our structural solution from X-ray data predicts a formula with slightly fewer than nine potassium cations per cluster, which along with the NMR and IR data lends support for the presence of framework hydroxyls. Because of the large range of $Nb-O_b$ bond distances (1.83−2.24 Å), we cannot determine absolutely which Nb_2O_b or Nb_3O_b sites are protonated, and they are most likely disordered.

Locations of K^+ and Water by Molecular Modeling. A structural model of the GeNb12-2d unit cell was constructed on the basis of the experimentally determined unit cell and replicated into a 2 × 2 × 1 supercell for the classical simulations. A rigid framework is utilized, where the lattice constants and Keggin chains are constrained to their crystallographically determined coordinates, while permitting the potassium cations and water molecules to move freely throughout the simulation cell with all of the symmetry constraints removed. The disorder of the framework O_c13 and O_c14 and O_b1 and O_b2 oxygen atoms is modeled by filling half of the positions with oxygen atoms and assuming that the populated positions will maximize their distance (O_b1-O_b2 and O_c13-O_c14, respectively).

First, the potassium cation distribution in the *dehydrated* GeNb12-2d structure was investigated to understand the energetically favorable binding sites created through interactions with the Keggin chain framework better. Because the locations of the protons are undetected through experimental techniques, charge neutrality is satisfied by randomly inserting 10 potassium cations per GeNb12-2d into the regions between the Keggin chains without any bias toward the experimentally observed sites. Canonical Monte Carlo simulations with periodic replica exchanges are conducted to sample configuration space efficiently and determine the preferred potassium cation distribution in GeNb12-2d. The replica exchange Monte Carlo simulations indicate that for the *dehydrated* system the experimental K1, K2, K3, K5, and K6 sites are essentially fully occupied with potassium. An interesting point to note from the analysis of the *dehydrated* structure is that 90% of the potassium cations are located near the experimentally determined sites, suggesting that these sites are stabilized by high coordination environments with the framework oxygen atoms of the Keggin chains. Observation of the coordination number with the framework oxygen atoms provides insight into the stability of these sites. The K1 potassium cations are positioned between two adjacent Keggin clusters, where each respective cluster contributes four Keggin oxygen atoms that frame a four-ring "window", giving an overall coordination number of 8 with a maximum distance of 3.2 Å. In fact, this position is considered "framework" when describing this phase as a layered structure. The K3 potassium cations are

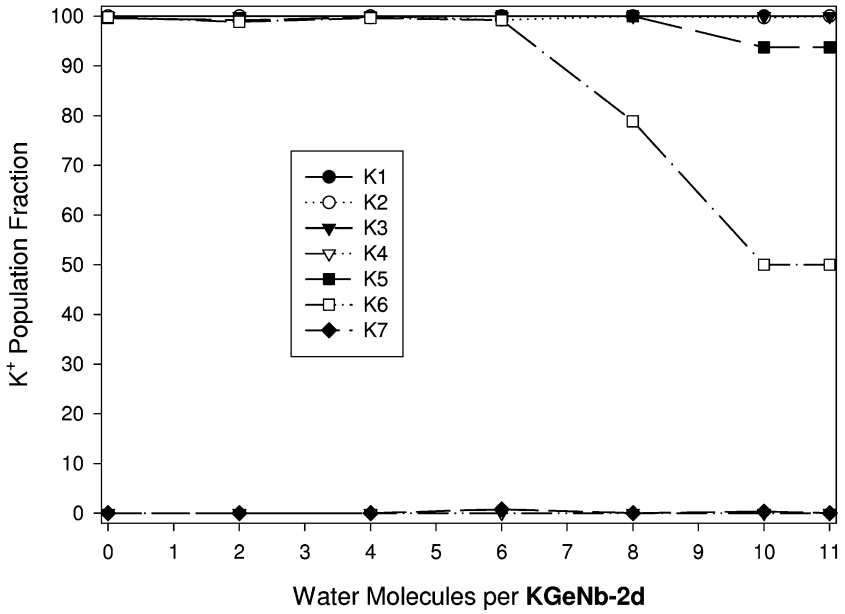

Figure 7. Simulated potassium population fraction as a function of water loading. Note that the symbols of K1, K2, K3, K5, and K6 are located on top of one another at low water loadings and at the ~100% population fraction. Additionally, the K4 and K7 symbols overlay one another at the 0% population fraction.

bonded to two terminal Nb═O_t oxygen atoms and two bridging Nb_2-O_b oxygen atoms. The K5 potassium cations are five-coordinated and are located near three terminal Keggin Nb═O_t oxygen atoms and two bridging Nb_2-O_b oxygen atoms. Finally, the K2 and K6 potassium cations are in symmetrically similar locations near the [Nb_2O_2] bridge between the Keggin ions. They coordinate with three terminal Keggin oxygen atoms and gain an additional 0.5 coordination from the disordered O_b1 or O_b2 oxygen atoms in the [Nb_2O_2] bridges.

Although the *dehydrated* structure provides valuable information regarding the preferred adsorption sites of potassium relative to the framework, the adsorption of water has been shown to lead to the *redistribution* of cation positions in similar materials, such as faujasite zeolites.[46] In the present study, water is systematically inserted into the lattice up to a maximum loading of 11 water molecules per Keggin chain. At each intermediate water-loading step, the system is equilibrated through replica exchange canonical Monte Carlo simulations, and the cation and water population fractions are analyzed. The analysis of the experimental potassium site population fraction as a function of water loading (Figure 7) shows the cation distribution to be essentially constant from loadings of 0−6 water molecules per Keggin chain. The K1, K2, K3, K5, and K6 sites remain essentially fully occupied with potassium. At these loadings, Figure 9 shows water to locate in the Ow3 site preferentially. In addition, water begins to populate the Ow1 and Ow2 sites.

At loadings greater than 8 water molecules per GeNb12-2d, a redistribution of the K6 potassium cations to the crystallographic position near (0, $^1/_2$, 0.031) is observed. Although this site is not observed experimentally, there is in fact residual electron density located at this proposed site. This is likely an artifact of the system, where all simulations were performed with 10 potassium cations per GeNb12-2d in order to meet charge-balancing requirements *without* adding framework protons. On average, the experimental K^+ loading per GeNb12-2d is lower than the model loading. As illustrated in Figures 7 and 8, water causes potassium to migrate from the K6 site to the (0, $^1/_2$, 0.031) position. As the water loading is increased to 11 water molecules per GeNb12-2d, enough water displaces potassium, where the K6 site becomes half-occupied with potassium and water, respectively. Further examination of the structure shows potassium to occupy the crystallographically equivalent K6 sites that maximize the coordination with the bridging O_b1 framework oxygen. Thus, the orientation of the bridging O_b1 framework oxygen will dictate the preferred potassium locations in the equivalent K6 sites.

Although there is excellent agreement with the half-occupied K6 site determined through X-ray diffraction, there is no computational evidence of potassium depopulating from the K2 site at saturated conditions. The computational model predicts half potassium occupancy at K6 and full occupancy at K2, whereas the experimental data describes both sites as half-occupied. Furthermore, there is no computational evidence of potassium populating the experimental K4 and K7 sites, which may be directly related to the fact that K2 remains fully occupied. Thus, water is observed to partially occupy the K4 and K7 sites instead of the Ow5 site observed experimentally. The simulated coordinates of the potassium cations and water molecules at saturation (11 water molecules per Keggin cluster) are compared to the experimental positions in Table 4. The magnitude of the standard deviation gives some indication of the relative mobility of a particular species. Overall, the computed potassium positions are in excellent agreement with experiment, where the cations located in K1, K2, K3, K5, and K6 positions deviate by less

(46) Beauvais, C.; Boutin, A.; Fuchs, A. H. *C. R. Chim.* **2005**, *8*, 485−490.

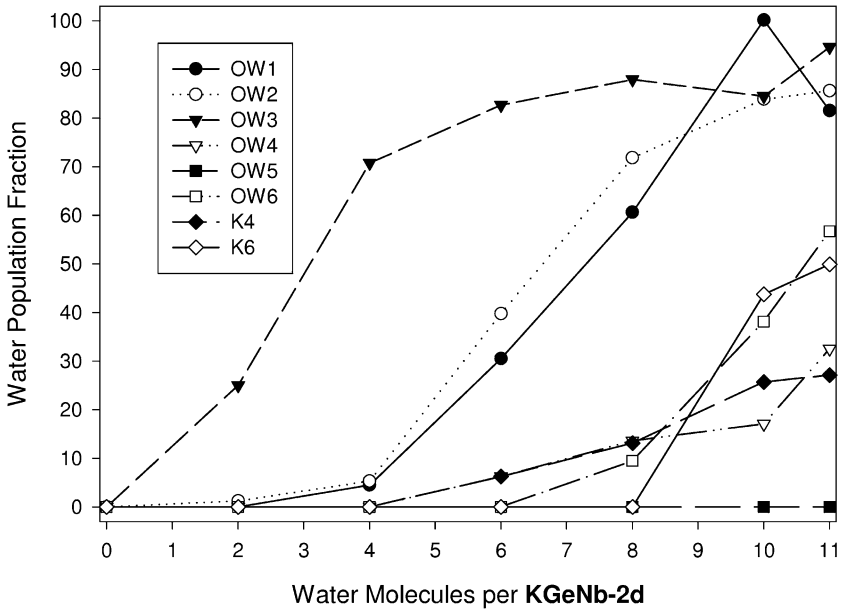

Figure 8. Simulated water population fraction as a function of water loading.

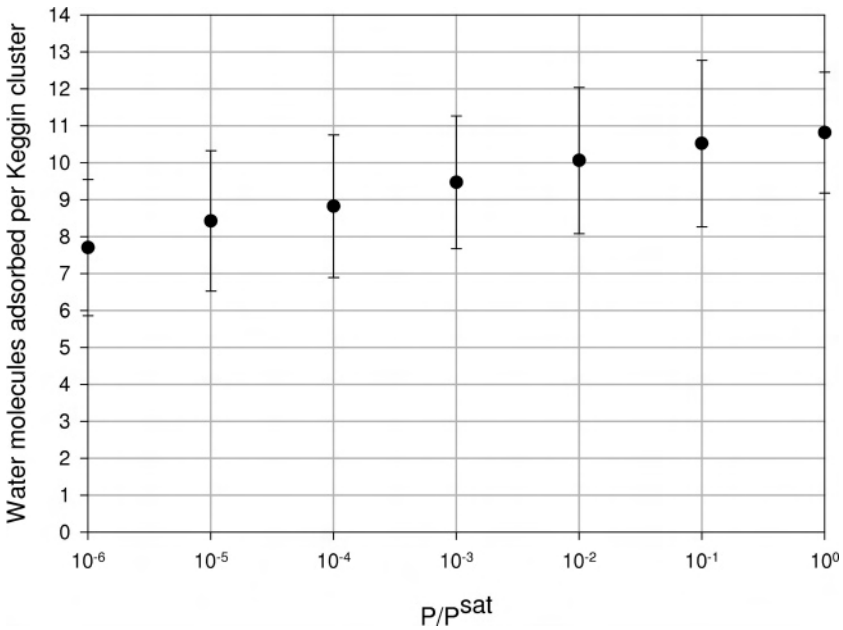

Figure 9. Simulated adsorption isotherm of water in GeNb12-2d at 300 K. Error bars are the standard deviation obtained through block averaging over all GCMC simulations at a given state point.

than 0.3 Å. The water molecules are significantly more mobile than the K^+ cations, given the consistently higher standard deviations shown in Table 4. Nonetheless, significant water populations are observed in most of the experimental water sites. The major source of disagreement between the simulation and experiment is noted to be with the disordered sites.

After each replica exchange Monte Carlo simulation, the final configurations at various water loadings are used as initial configurations for the GCMC simulations. The GCMC simulations are performed at seven state points to obtain the adsorption isotherm. An averaged isotherm is then obtained by block averaging over all GCMC simulations at a given state point. The block-averaged adsorption isotherm is given in Figure 9. The isotherm shows the hydrophilic nature of the GeNb12-2d system, where water easily adsorbs and solvates the potassium cations at very low partial pressures of water. At saturation, a total water loading of 10.8 ± 1.6, corresponding to a weight loss of $7.4\% \pm 1.0\%$, is observed, which is in excellent agreement with experimental estimates of 11 water molecules per GeNb12-2d from both X-ray structure and thermogravimetry.

Summary and Conclusions

In this article, we have presented structural and spectroscopic characterization of a new phase featuring $[GeNb_{12}O_{40}]$ Keggin ions linked in two dimensions, with interstitial, exchangeable water molecules and potassium cations. The mobility and disorder of these extraframework species renders them difficult to characterize, and therefore their

Table 4. Coordinates of K^+ and H_2O in GeNb12-2d[a]

species (exptl site)		*x*	*y*	*z*	dev. (Å)	std dev. (Å)	pop. frac./occupancy[b]
K^+ (K1)	raw:	0.500	0.500	0.317	0.11	0.16	100.0%/100%
	ideal:	$^1/_2$	$^1/_2$	0.317	0.11		
K^+ (K2)	raw:	0.164	−0.001	0.151	0.10	0.27	100.0%/50%
	ideal:	0.164	0	0.151	0.10		
K^+ (K3)	raw:	−0.003	0.180	0.985	0.28	0.16	100.0%/100%
	ideal:	0	0.180	0.985	0.28		
K^+ (K4)	raw:		not observed				0%/50%
	ideal:						
K^+ (K5)	raw:	0.000	0.187	0.633	0.12	0.20	93.8%/100%
	ideal:	0	0.187	0.633	0.12		
K^+ (K6)	raw:	0.163	0.000	0.485	0.20	0.14	50.0%/50%
	ideal:	0.163	0	0.485	0.20		
K^+ (K7)	raw:		not observed				0%/38%
	ideal:						
H_2O (Ow1)	raw:	0.019	0.505	0.592	0.78	0.72	81.5%/100%
	ideal:	0	$^1/_2$	0.592	0.78		
H_2O (Ow2)	raw:	0.322	0.168	0.489	0.36	0.88	85.6%/100%
	ideal:	0.322	0.168	0.489	0.36		
H_2O (Ow3)	raw:	0.298	0.191	0.105	0.27	0.89	94.6%/100%
	ideal:	0.298	0.191	0.105	0.27		
H_2O (Ow4)	raw:	0.424	−0.015	0.198	0.70	1.29	32.5%/50%
	ideal:	0.424	0	0.198	0.68		
H_2O (Ow5)	raw:		not observed				0.0%/100%
	ideal:						
H_2O (Ow6)	raw:	0.503	−0.048	0.415	0.75	1.25	56.8%/100%
	ideal:	1/2	0	0.415	0.50		
H_2O (K4)	raw:	0.382	0.001	0.433	0.97	0.25	27.1%/0%
	ideal:	0.382	0	0.433	0.97		
H_2O (K5)	raw:	0.014	0.217	0.675	0.81	0.51	6.2%/0%
	ideal:	0	0.217	0.675	0.80		
H_2O (K6)	raw:	0.158	0.004	0.471	0.18	0.31	50.0%/50%
	ideal:	0.158	0	0.471	0.18		

[a] The simulated raw averaged and simulated idealized coordinates are given for comparison. The idealized coordinates shift the raw coordinates onto nearby, higher-symmetry special positions. The average deviation and standard deviation are given for comparison with X-ray diffraction experiments, which give an indication of the strength of adsorption and relative mobility associated with each respective site. [b] Population fraction is derived from the computational study and describes the percentage of time the site is occupied by the species of interest. The occupancy is derived from the crystallographic data.

location and behavior were investigated by multiple experimental and computational approaches. Thermogravimetry, X-ray data, and modeling all gave excellent agreement in the number of lattice waters per formula unit, and D_2O exchange and spectroscopic studies provided information on the mobility of the water molecules occupying the different crystallographic sites. We observed agreement between experimental and simulated location and bonding geometry for the majority of the potassium and water sites. These studies thus validate the computational method for reasonably accurate prediction of mobile cations and water molecules in open-framework phases. Disagreement between computational and experimental models was primarily associated with disordered crystallographic sites within the crystalline lattice. However, prediction of K^+ bonding to the framework utilizing the basicity of the different framework oxygen sites using DFT calculations proved quite accurate. Furthermore, K^+ cations bonded predominantly to lattice water were also accurately predicted by the simulations. Thus, we are moving toward a computational method that can potentially be a powerful predictive tool for understanding the behavior of ion-exchange materials without the benefit of an accurate experimental structure, as is often the case with high-surface-area ion exchangers that exhibit poor long-range order or can be obtained only as microcrystalline powders. We are currently investigating a computational model of $K_{12}[Ti_2O_2][SiNb_{12}O_{40}]\cdot 16H_2O$,[27] a Keggin-chain phase *without* disorder in the framework to provide further validation of our computational models and methods.

Acknowledgment. This work was funded by the Department of Energy, Office of Environmental Management, by grants from the Office of Cleanup Technologies and the Office of Biological and Environmental Research in the Office of Science, by a grant from the Environmental Management Science Program, and Sandia National Laboratories LDRD program. Sandia National Laboratories is a multiprogram laboratory operated by Sandia Corporation, a Lockheed Martin Company, for the U.S. Department of Energy's National Nuclear Security Administration under contract DE-AC04-94AL85000. H.P. thanks Dr. Y.-S. Chen at ChemMatCARS, Advanced Photon Source, for assistance in collecting single-crystal diffraction data. ChemMatCARS Sector 15 is principally supported by the National Science Foundation/Department of Energy under grant number CHE-0087817. The Advanced Photon Source is supported by the U.S. Department of Energy, Basic Energy Sciences, Office of Science, under contract no. W-31-109-Eng-38. SUNY-SB acknowledges grants NSF-CHE-0221934 (CEMS) and NSF-DMR-0452444 for funding. We thank Todd M. Alam (Sandia) for the ^{1}H MAS NMR spectroscopy.

Appendix

Replica Exchange Monte Carlo Simulations. In previous studies,[26,47] we used a simulated annealing molecular dynamics protocol to overcome deep energy wells that are typically present in crystalline systems. In this approach, the system was heated to higher temperatures (in the theoretical sense) and systematically quenched to low temperatures. In the present work, replica exchange Monte Carlo (REMC) simulations[46,48−50] are utilized to probe configuration space efficiently, where canonical ensemble (constant number of atoms, volume, and temperature, or NVT) Monte Carlo simulations are performed independently and simultaneously on multiple processors at various temperatures. Periodically, attempts are made to swap the configurations of simulations at "adjacent" temperatures. The probability of acceptance for the swap attempts from state m to state n is governed by the expression

$$\Pi_{\text{swap}}^{mn} = \min[1,\exp(-(\beta_m - \beta_n)(U_n - U_m))] \qquad (2)$$

where $\beta_m = 1/(k_B T_m)$, k_B is Boltzmann's constant, T_m is the temperature of state m, and U_m is the potential energy of the system at state m.

A total of 16 independent realizations of the system are simulated, each one at a constant NVT_i, where T_i represents the temperature of processor i. Intermediate temperatures are chosen to ensure swap acceptance rates of at least 3% between adjacent processors. In this system, a T_{i+1}:T_i temperature ratio of 1.1−1.2 satisfied the acceptance rate criteria, depending on the water content. In replicating the system over 16 processors, the temperature ranges from 300 to 2440 K. As the water loading increased, the T_{i+1}:T_i temperature ratio was decreased to 1.1, giving a temperature range of 300−1250 K over 16 processors. Note that the high-temperature simulations are not necessarily physically reasonable in an experimental sense but are used to improve the sampling of configurational space. The predicted properties of the system are computed from the 300 K realization.

To investigate the preferred adsorption sites and the influence of water on potassium cation distribution, water is systematically added to the system followed by a sequence of replica exchange Monte Carlo simulations. To begin, 10 potassium cations per GeNb12-2d are randomly inserted into the *dehydrated* structure. Canonical Monte Carlo simulations with periodic replica exchange attempts every 100 Monte Carlo steps are performed for a total of 30 million Monte Carlo steps to equilibrate the *dehydrated* system and determine the preferred cation distribution. Next, a predetermined amount of water is randomly introduced into the system, and another 30 million Monte Carlo steps with replica exchanges are performed to determine the preferred cation and water distributions. The actual water loadings simulated are thus 0, 2, 4, 6, 8, 10, and 11 water molecules per GeNb12-2d. For the $N = 7$ intermediate steps, each having a different water loading, a replica exchange Monte Carlo simulation is conducted, and the cation and water distribution is examined.

Grand Canonical Monte Carlo Simulations. Grand canonical Monte Carlo (GCMC) simulations[41] are used to compute the equilibrium water adsorption in GeNb12-2d. In standard GCMC simulations at 300 K, the water loading may increase rapidly as the simulation comes to equilibrium, which may lead to cations becoming trapped in locally stable positions that are highly dependent on the initial configuration. This makes thermal equilibration moves difficult to carry out for the cations, leading to poor sampling. By slowly adding water to the system and applying the REMC algorithm, the cations and water molecules are able to redistribute and explore the most favorable configurations. This is the reason that REMC was used to improve sampling of the *NVT* MC simulations. Thus, to compute isotherms for this system, a combined GCMC/REMC algorithm was used.

After obtaining the equilibrated structures from REMC simulations at each water loading, we conducted GCMC simulations for 20 million Monte Carlo steps, where each step consists of one of four possible Monte Carlo moves: cation and water translations, water rotations, and water insertions and deletions. In this work, translations and rotations were each attempted 45% of the time, whereas insertions and deletions were each attempted 5% of the time. To improve insertion efficiency and speed convergence, a configurational biasing algorithm was implemented, where a water molecule is inserted through a combination of energy and orientational biasing moves.[50]

Initial configurations for the GCMC simulations are obtained from the final configurations of the REMC simulations conducted at $N = 7$ different water loadings. The adsorption isotherm at 300 K is evaluated for each of the $N = 7$ initial configurations through GCMC simulations. Seven state points on the adsorption isotherm are computed. The saturation pressure of water at 300 K is approximately 3.56 kPa. Thus, the ratio of the gas-phase pressure to the saturation pressure (P/P_{sat}) is varied from 10^{-6} to 1.0, increasing the gas-phase pressure by an order of magnitude for each intermediate-state point. Finally, an averaged isotherm is obtained by block averaging the number of adsorbed water molecules over $N = 7$ GCMC simulations for each state point. The statistical error associated with each state point is also computed by determining the standard deviation at each state point.

Supporting Information Available: Crystallographic information file for GeNb12-2d. This material is available free of charge via the Internet at http://pubs.acs.org.

IC061454L

(47) Larentzos, J. P.; Clearfield, A.; Tripathi, A.; Maginn, E. J. *J. Phys. Chem. B* **2004**, *108*, 17560−17570.
(48) Faller, R.; Yan, Q.; Pablo, J. J. d. *J. Chem. Phys.* **2002**, *116*, 5419−5423.
(49) Kofke, D. A. *J. Chem. Phys.* **2002**, *117*, 6911−6914.
(50) Macedonia, M. D.; Maginn, E. J. *J. Mol. Phys.* **1999**, *96*, 1375−1390.